Visco-elasto-plastic characterization and modeling of a wet polyamide laid-strand sub-rope for floating offshore wind turbine moorings

Laure *Civier*[a,b,c], Yoan *Chevillotte*[a], Guilhem *Bles*[a], Guillaume *Damblans*[c], Frédéric *Montel*[a], Peter *Davies*[b,c], Yann *Marco*[a]

[a] *UMR CNRS 6027, IRDL, ENSTA Bretagne, 2 Rue François Verny, Brest, 29200, France*
[b] *IFREMER, Marine Structures Laboratory, 1625 Rte de Sainte-Anne, Plouzané, 29280, France*
[c] *France Energies Marines, 525 Av. Alexis de Rochon, Plouzané, 29280, France*

Abstract

Polyamide 6 fiber ropes are of interest for floating offshore wind turbine mooring lines but could exhibit complex mechanical behavior during loading at sea, such as creep, relaxation, variable dynamic stiffness or visco-plasticity. There is a need for a model that could be introduced into finite element analyses in order to predict this complex response. It should also describe the effect of the loading history. This paper proposes an elasto-visco-plastic behavior model based on four dashpot-ratchet-spring elements that allow a precise description of polyamide 6 rope behavior. An identification method, using a multi-relaxation test, is described. It has been implemented in a finite element and validations are made by comparing the model results to the experimental data. The present work is the result of an extensive effort initiated by the 3-year collaborative research project POLYAMOOR and continued by the MONAMOOR project, both led by France Energies Marines.

Key-words: polyamide 6, constitutive model, synthetic rope, laid strand

1. Introduction

Offshore floating wind turbines will be located in exposed sites with significant environmental loading due to waves and wind. They will require mooring lines that maintain the floater position and withstand the swell energy (Davies *et al.* 2003; Flory *et al.* 2007). Synthetic fiber ropes have become extremely attractive as an alternative to steel chain and wire ropes due to their light weight, easier handling for installation and the possibility to reduce the overall footprint. The high compliance and viscosity of synthetic ropes will lower the line tension and provide damping. Polyamide 6 (PA6) fibers are well-suited for this type of application thanks to their low stiffness, good tensile strength and their

viscous behavior. Polyester mooring lines could be used but their stiffness remains too high to withstand the structural load of the floater. Polyamide 6 ropes are already used in other marine applications but their visco-elasto-plastic behavior is not fully understood, and they are limited to temporary applications. The development of a reliable model for the mechanical behavior of polyamide 6 fibers is essential for permanent mooring applications. It should allow the strain and the stress to be predicted as a function of the loading history and it should satisfy the hypotheses and rules of finite element (FE) simulations. This paper proposes a constitutive law called 'POLYAMOOR law' that aims at completely describing the complex behavior of polyamide 6 fiber elements. The identification of the parameters of this law allows a visco-elasto-plastic characterization of the complex mechanical response of polyamide ropes. The model has been implemented in a commercial finite element code; the present study shows first comparisons between the model and experimental results for a laboratory rope scale.

The following section will discuss first the complex behavior of polyamide 6 ropes due both to their fiber structure and properties, and also to their hierarchical organization and construction. It will then present existing models, that have been developed to investigate the complex behavior of synthetic ropes more generally.

1.1. Structure and complex behavior of polyamide 6 fibers

Polyamide 6 fibers, and more broadly, synthetic fibers, are characterized by a time-dependent load-elongation behavior and a non-linear viscoelastic and viscoplastic behavior (Chailleux and Davies, 2005). The behavior of a nylon 6 rope is characterized by an elongation under a constant load called 'creep' or a load drop under constant strain known as 'relaxation', characteristic of a time dependent viscous behavior; it is also characterized by hysteresis during cyclic loading, that highlights the ability to absorb and dissipate energy; it can show a permanent extension after initial loading of a new rope, characteristic of a viscoplastic behavior and a construction rearrangement of the rope (Weller *et al*., 2015). This complex behavior is due to both the polymeric nature of the filaments and also to their hierarchical structure and construction.

In addition, the mooring line application requires knowledge of the behavior of polyamide 6 fibers in water. Humeau *et al* showed that these fibers are very sensitive to water (Humeau *et al*., 2018). A significant water uptake is noted during immersion, which induces a plasticizing effect, so the experimental identification of the model parameters must be performed on wet samples.

1.2. Effect of scale and construction

The visco-elasto-plastic behavior of ropes for mooring lines is mainly the result of the material properties of polyamide 6 fibers. However, the effects of the rope construction must also be considered as they play a major role in the stabilization of the whole structure when the rope is first loaded (François and Davies, 2008). The main parameters influencing the behavior for twisted rope will be its lay-length and the twist angles. Lechat *et al* studied different components of a twisted polyester rope. They showed that a similar nonlinear behavior was observed at all scales, but the higher scale presented a loss of strength and modulus. For that twisted structure, this loss was related to the number of fundamental elements and the twisting angle (Lechat *et al.*, 2006).

1.3. Different model of ropes materials

The design of mooring lines has been the main motivation to develop models that describe the complex non-linear behavior of synthetic ropes. Since lines are already in service offshore, guidance documents have been proposed (François and Davies, 2008). Dynamic stiffness tests are often employed for the characterization of rope behavior. The dynamic stiffnesses are measured by cyclic loading around a mean value. Apparent spring constants are determined, and viscoelastic parameters can be analytically calculated to implement three-parameter models (Lechat *et al.*, 2006). Currently in the offshore industry, the viscoelastic and viscoplastic behavior of mooring lines is accounted for by stiffness values related to two tension load cases, quasi-static and dynamic. The latter is due to the response of lines under wave loading or under the movements of the platform. This description is very limiting when designing offshore floating wind turbine floaters and mooring lines as they will be subjected to more complex constraint. They are expected to maintain the integrity of the electricity export cable, limit the floater offset, withstand the wave loading and they should not lose too much tension (creep effect) during their service life (which would require maintenance for re-tension). Hence, to be able to design properly and precisely these complex structures and their response, there is a need to introduce a model describing the complex behavior of polyamide 6 mooring lines that could also describe the effect of the history of these loadings on the rope's response.

Various approaches for modeling the behavior of synthetic fibers are proposed in the literature. They are distinguished by their consideration of the fiber structure. For a macro-mechanical approach and direct treatment of experimental data, continuum and micro (or meso) mechanical models are well-suited. A mechanical approach proposed by Ghoreishi *et al* (Ghoreishi *et al*., 2007) assumes the complex hierarchical structure as a continuum formed by a set of coaxial helixes only characterized by their external angle and corresponding radius. In this approach the constitutive material is assumed to be linear and the inter-fiber friction effects are neglected. By contrast, Durville *et al* (Durville, 2002) proposed a meso-mechanical approach with a description of contact-friction interactions between

beams in large transformations. The aim was to model the behavior of fiber structures by considering the contacts at the mesoscopic scale between the base components (fibers or yarns). In these approaches, the complex non-linear visco-elasto-plastic behavior of polyamide 6 fibers is not considered. In our case, phenomenological models, which consider the fibers as a homogeneous nonlinear viscoelastic body are more suitable.

François and Davies (François and Davies, 2008) proposed a model which defines the rope properties with several separate terms in order to simulate the behavior of PET ropes. These terms correspond to different responses of the rope:

- A mean elongation (system pretension and permanent load),
- A visco-elastic response due to slow variation of mean load, which is modelled by a quasi-static stiffness,
- A dynamic response which is modelled by the dynamic stiffness and depends on the mean load

The quasi-static stiffness defined by François is determined using a cyclic test between two chosen tension levels with a constant load plateau at each level during which creep and recovery occur. This model consists of the summation of three strains: one for the fully relaxed behavior, one for the non-recoverable strain and one for the viscoelastic behavior. Therefore, the rope strain is a function of both the current tension and the maximum tension undergone by the rope (this approach provided a good description of the polyester rope behavior observed experimentally). François and Davies considered that a fully relaxed behavior exists for an 'infinitely slow 'rate of loading. The advantage of this approach is that it can be used in current mooring line software.

Recent studies from Huntley on a wire-lay-3-strands nylon rope showed that the dynamic stiffness of the nylon rope depends on both the applied mean tension and the tension amplitude (Huntley, 2016). Hence, Pham *et al* (Pham et al., 2019) proposed a practical mooring analysis procedure to capture the tension amplitude effect on the dynamic mooring analysis. In this procedure, an empirical expression of the dynamic stiffness that considers the mean tension and the tension amplitude for nylon is used.

One of the first macroscopic quantitative models for mooring ropes was proposed by Chailleux and Davies to describe the creep and recovery behavior of polyester and aramid fibers (Chailleux and Davies, 2005). It is an adaptation of Schapery's non-linear viscoelastic and viscoplastic constitutive model (based on the modification of the generalized Boltzmann integral). This work was continued by Huang *et al* who employed Schapery's single integral constitutive model to describe the viscoelastic

behavior and a one-dimensional dashpot-slider-spring model to represent the viscoplastic behavior (Huang *et al.*, 2015, 2013).

Falkenberg *et al* then developed the 'Syrope' model to describe the tension-stretch and axial stiffness characteristics of polyester ropes (Falkenberg *et al.*, 2017). It is based on experimental testing. This model consists of:

- An original curve which represents the tension versus elongation during the first loading of a new rope,
- The original working curve, corresponding to the stationary working point if the rope is at its historical highest mean tension and when the permanent stretch has been taken out,
- The working curve which represents the working point when the curve is at a lower mean tension than the preceding maximum mean tension.

Sorum *et al* proposed using the Syrope stiffness and the bi-linear stiffness model to predict fatigue lifetime of polyester mooring lines (Sorum et al., 2023). In their study, the Syrope model accounts for the quasi-static stiffness and permanent rope elongation while the bi-linear model applies both the quasi-static and dynamic stiffness in the dynamic analyses.

Flory *et al* developed a spring and dashpot model aiming to describe the complex change in-length characteristic of polyester ropes (Flory *et al* 2007) (Figure 1). Their model integrates the visco-elasto-plastic behavior of the material as well as the construction response that will include twisting, elongation, friction, packing and locking, which Flory called the 'construction stretch'. This model is phenomenological and does not aim at representing the actual components of the rope. The model is composed of four units in series:

- The creep, associated to polymer stretch, represented by the separate dashpot unit (4),
- A parallel spring and ratchet unit represents the construction stretch (3),
- A parallel spring and dashpot unit represents the slow response to tension and is associated with the working stretch (2),
- A separate spring unit represents the fast response to tension and is responsible for the dynamic stretch (1).

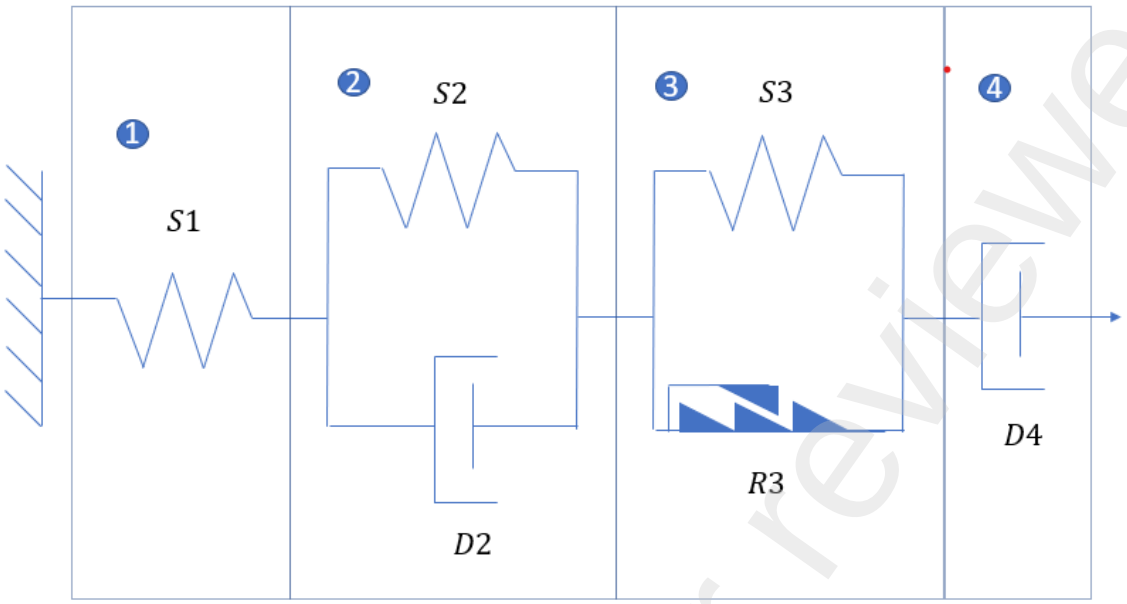

Figure 1 - Flory's spring and dashpot model (based on Weller et al., 2018)

In that work, the equations of the model were not detailed, and no simulation was shown. Weller *et al* (Weller *et al*., 2018) published a paper on a preliminary study on the identification parameters of the different elements of Flory's model. They considered a fully bedded-in rope that would not have any further significant construction stretch. Therefore, they chose to take out the parallel spring dashpot unit leading to a four-parameter Burger model. This simplified model allowed the change-in length of the rope to be examined but was not sufficient to fully represent the complex time-dependent behavior.

The present paper proposes a constitutive model based on Flory's proposal (Figure 1). Its development is based on the characterization of a polyamide 6 sub-rope in water and under representative conditions for different loadings. The identification method is direct and does not use any inverse identification approach as Weller *et al* did. This allows more control over the model. This phenomenological model aims to describe the real behavior of the rope during loading at sea, and to be implementable in the one-dimensional finite element analyses used in industry (using software such as ®Deeplines, ®Orcaflex, ®Flexcom, ®Sima …).

2. Materials and methods

2.1. Materials

The synthetic rope studied is a reduced scale of a polyamide sub-rope for mooring lines supplied by Bexco, Hamme Belgium. The reduced-scale sub-rope studied in this paper was specially manufactured

for the research project. It was tested in the form of 1-meter-long (pin-to-pin) three-stranded rope samples with a diameter of around 11.5 mm, an MBL of 40 kN and a linear density of 90 000 tex (g/km); it will be referred in this paper as '4Tsample'. Each strand is composed of yarns twisted together into rope-yarns. The rope-yarns are twisted together to form strands.

The yarns used were supplied by Nexis fibers and have a linear weight of 188 tex (g/km). A proprietary coating has been applied on the rope-yarns by the rope manufacturer Bexco. This coating aims to reduce the abrasion inside the rope improving its fatigue durability (the target fatigue lifetime for FOWT is 20 years) (Chevillotte, 2020).

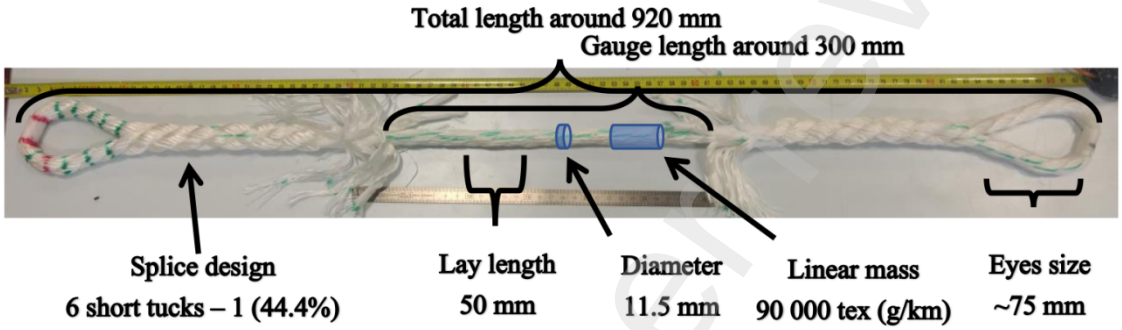

Figure 2 - 4T sub-rope sample with splices

The development of the behavior law was performed on this 4T sub-rope sample. This smaller scale is more adapted to laboratory experiments and the splices could be prepared in the laboratory at ENSTA according to Bexco practice. This allowed more experiments to be performed as the cost was also reduced. Several rope samples were needed to develop and identify the parameters of a behavior law and to validate the model predictions.

An example of the 4T sub-rope samples is presented in Figure 2. All samples were terminated by eye splices in order to be connected to the tensile testing machine. The strand lay-length imposes the length of the splices.

Before each test, the sub-rope samples were fully immersed in tap water for 10 hours without load, in order to saturate them. As shown by (Humeau *et al*., 2018) on the same fiber type but without coating, this duration should be largely sufficient. During the tensile tests, the samples were maintained under water as explained in the next section.

2.2. Experimental procedure: monotonous tensile test, multi-relaxation tests and multi-creep test

Testing polyamide 6 sub-ropes requires adapted test machines and load introduction interfaces. First, the recommended terminations for ropes are splices as noted in *section 2.1*. These terminations result in long samples (fig. 2). Hence, the experimental machine should be long enough to hold the sample and provide enough stroke to accommodate the elongation of the sample during the test. The latter is important as polyamide 6 shows a low stiffness with a high breaking strain around 20%. Adding the construction stretch to the high elongation fibres and to the splice terminations, a large displacement stroke is required for testing these ropes. A hydraulic machine dedicated to compression tests at high rates (Figure 3-left) called 'Servotest' fulfilled these requirements. This Servotest machine may be also used for quasi-static tensile test, having a large piston stroke of 600 mm. The maximum displacement speed is 100 mm/s for quasi-static tests. The maximum tensile force is 200 kN at 10 m/s. The sample splices are linked to the machine by two 35-mm diameter loading pins.

Figure 3 - Left: Servotest hydraulic machine at ENSTA Bretagne; Right: 4T sub-rope samples attached to the jaws with vertical watering system

This is a vertical test machine. As noted previously the experimental tests must be performed in water. Following immersion in water for 10h the samples were kept wet during the test by a vertical system producing a constant and controlled water flow around the sub-rope. This consists of a volumetric pump with a low flow rate (around 1liter/min) that brings tap water near the top of the sample through a spiral-shaped pierced tube covered by a knitted fabric (Figure 3-right). This provides a homogeneous flow around the sub-rope section. The water then flows along the sample length by gravity. The lower loading pin is surrounded by a PVC tube for collecting the sample water and returning it to a tank. The HBM load cell has a range of ±50 kN and a resolution of 2 mV/V leading to a precision of around 10 N. The strain, in the central part of the sub-rope samples, was measured by

image analysis; two black 2mm-diameter markers were attached to the sub-rope and tracked by a CCD camera (Retiga 6000 by Q-IMAGING with 6.05 Mega Pixels).

2.3. Stress and strain measurements adopted

The complex structure of synthetic fiber ropes complicates the use of the usual Cauchy stress based on the cross-section. A specific stress tensor $\tilde{\Sigma}$ based on the density of the material is therefore used:

$$\tilde{\Sigma} = \frac{\tilde{T}}{\rho_t} \quad (1)$$

with ρ_t the density in kg/m³ and $\tilde{\mathrm{T}}$ the Cauchy stress tensor in Pa.

In the 1D case (rope case), this specific stress leads to:

$$\Sigma = \frac{F}{\overline{\overline{\rho_t}}} \quad (2)$$

with $\overline{\overline{\rho_t}}$ the linear density in kg/m and F the tensile force in Newton.

The SI specific stress unit is N.m/kg (= J/kg). The textile industry uses a specific unit called N/tex with:

$$1\,\frac{N}{tex} = 10^6\,\frac{J}{kg} = 10^3\,\frac{Pa}{g/m^3} \quad (3)$$

where 1 tex = 1 g/km.

For defining and measuring a strain, one needs a reference mechanical state, which defines the reference length L_0. In the case of rigid materials like metals, this reference state is usually chosen at rest, before any loading. In the case of textile materials, the mechanical state at rest, i.e., without any loading, has very variable geometric dimensions. Indeed, without any loading, this type of material has very low rigidity and we can easily modify its dimensions during handling. So, the state at rest cannot be used as a reference mechanical state, because of the high uncertainty of the reference length L_0. In order to overcome this difficulty, a simple solution is to apply a low load to the material in order to stabilize its dimensions. Then, this lightly-loaded mechanical state can be used as a reference state for L_0. This load rate is chosen as the minimum tension ensuring a straight rope under gravity.

The logarithmic strain will be used for this study:

$$\varepsilon_{log} = \log\left(\frac{L}{L_0}\right) \quad (4)$$

with L the current length, L_0 the reference length (measured with the rope loaded at 2% of its minimal breaking load or MBL) and $\log$ the natural logarithm.

2.4. Bedding-in procedure

For station-keeping applications, a bedding-in process is performed to stabilize the properties of the rope. It consists of a procedure with a chosen sequence of loading to allow the permanent strain, due to construction modifications and reorientations of amorphous regions of fibers, to take place before the installation. Lian *et al* (Lian, 2018) showed that, depending on the bedding-in applied to a rope, different values of strain, initial creep and stiffness could be observed. Bain *et al* (Bain *et al*., 2020) studied the influence of bedding-in loading on HMPE braided rope performance and showed that applying a pre-load of at least 30% of the break load improved the rope properties. Depending on the rope material and construction, appropriate loading procedures must be found, but recommendations are proposed, for example, by (NI 432 Dt R02 E Bureau Veritas, 2007) . After removing this construction effect, simpler models can be proposed for ropes.

Here a pre-loading sequence proposed specifically for the project is described in *Table 1*. It was applied with the loading rate equivalent to the ISO test.

Table 1 Bedding-in sequence performed before each test

Loading/unloading rate	Loading value [N/tex (%MBL)]	Creep/recovery duration [s]
$5 \cdot 10^{-4} s^{-1}$	0.07 (14)	3600
$-5 \cdot 10^{-4} s^{-1}$	0.01 (2)	3600

These two steps were applied for all tensile tests. The mechanical state at the end of this pre-loading is defined as the reference state for all strain measurements.

2.5 Multi-relaxation cyclic tests

Four identical multi-relaxation tests were performed on four different 4T sub-rope samples to investigate the viscoelastic and viscoplastic properties of the polyamide 6 sub-rope. The procedure applied to each sample includes cyclic loading, relaxations, recoveries and a complex loading history with various maximum loading states. This enables most of the elasto-visco-plastic behavior can be described. It consists of a sequence of load-unload cycles mixed with stress-relaxation stages. The procedure is shown schematically in Figure 4 and for the 4T sub-rope can be described as follows:

- Cyclic loading at a strain rate around $8 \cdot 10^{-5}\, s^{-1}$ (0.08 mm/s)

- Relaxation of 1 hour (by maintaining the piston position) at different strains during the cyclic loading

These tensile tests were preceded by the bedding-in procedure described previously. They were performed on the Servotest machine shown in Figure 3.

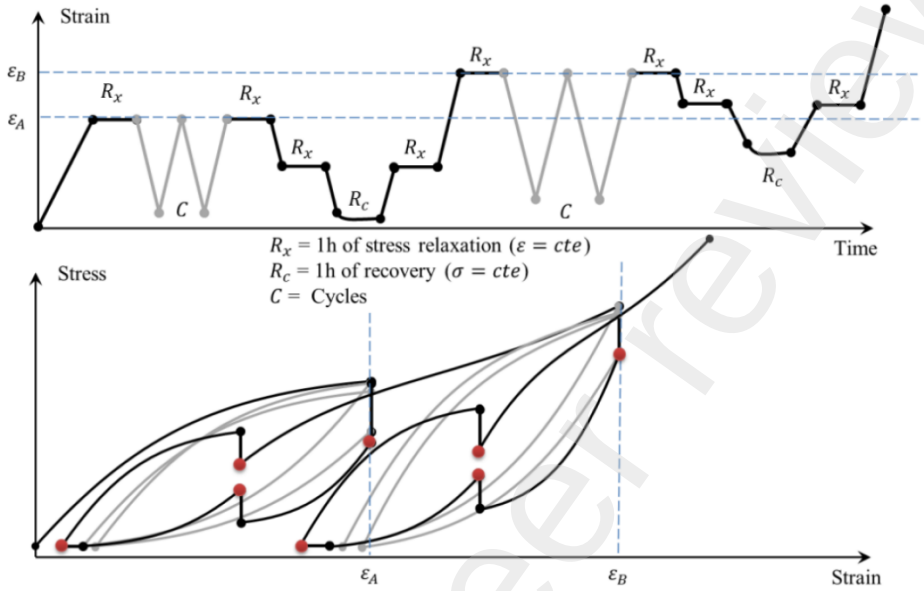

Figure 4 - Scheme of the loading paths of the multi-relaxation tests

3. Characterization of the behavior using multi-relaxation results and proposal of a constitutive law for a wet polyamide sub-rope

In this section, a visco-elasto-plastic characterization method is proposed. It is based on the analysis of the experimental results of multi-relaxation tensile tests (Figure 4 *in section 2.5)*. An example of the

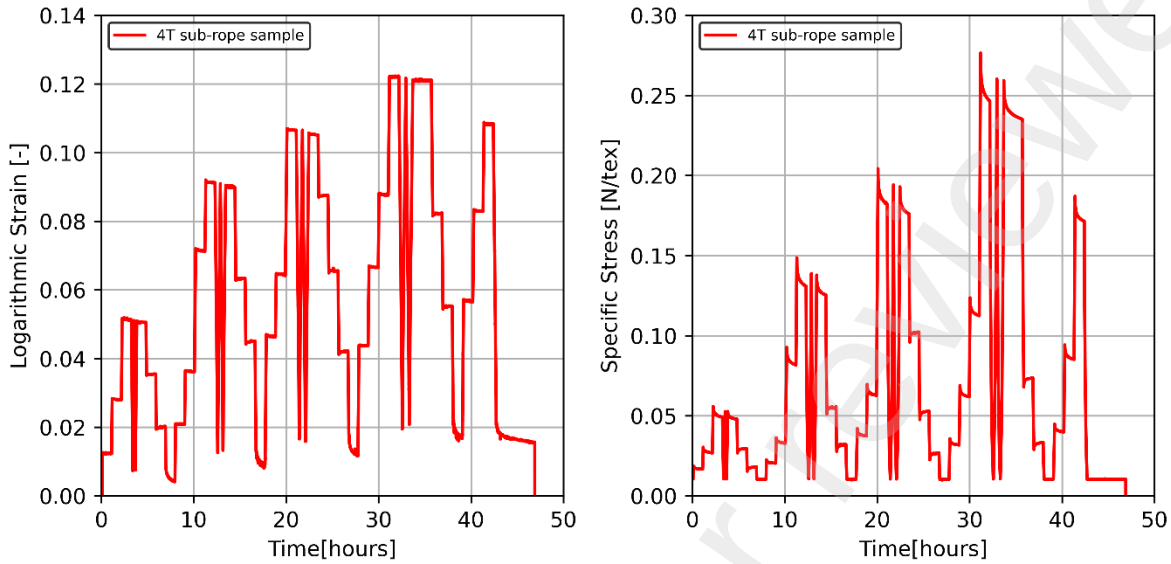

Figure 5 – Left: Strain versus time of a 4T sub-rope sample during multi-relaxation test. Right: Specific Stress of a 4T sub-rope sample during multi-relaxation test

experimental results from this type of test is shown in Figure 5. This characterization provides the identification of a visco-elasto-plastic behavior law based on Flory's model as described in *section 1.3*.

The one-dimensional spring-dashpot-ratchet law is represented in Figure 6 and has the following elements:

- A fast spring describing the dynamic behavior,
- A dashpot responsible for the viscous stress of the polymer,
- A time-independent part consisting of a ratchet element for the plasticity, and a slow spring responsible for the relaxed elasticity.

This proposed law does not represent the construction stretch and the stabilization of the amorphous region, assuming that the bedding-in procedure has been previously applied.

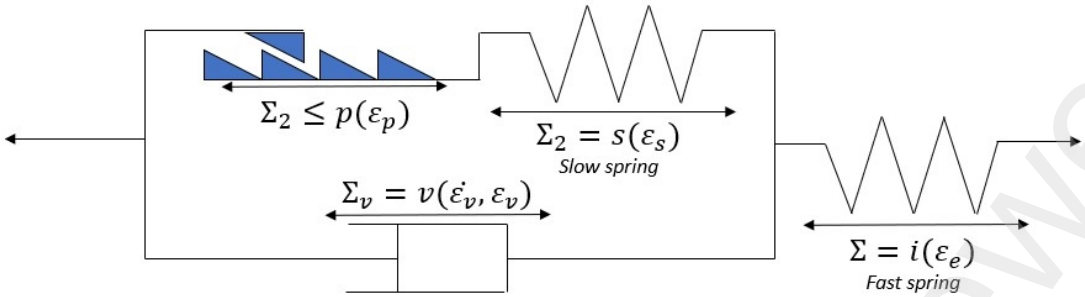

Figure 6 - The proposed constitutive law; POLYAMOOR model.

Two major hypotheses led to this model. First, the separate dashpot D_4 in Flory's model (Figure 1) was removed by considering that a fully relaxed state exists, which means a stabilized state at the end of all creep and relaxation (François and Davies assumption (François and Davies, 2008)). Second, we observed that the dynamic elasticity modulus is a linear function of stress (see next *section 3.1*). Therefore, it is not affected by the history of loading. The dynamic behavior of Flory's model is revealed by replacing dashpot D_2 by a rigid link; the resulting behavior is not exclusively elastic because of the position of the ratchet element in Flory's model. So, in the proposed law, the ratchet element is put in parallel with the dashpot (Figure 6). Therefore, the dynamic behavior is exclusively given by elastic spring 'i' (fast spring) and is not history dependent.

We can notice that this model is similar to the Syrope model presented in *section 1.1.3* (Falkenberg *et al.*, 2017) as it can describe the dynamic stiffness thanks to the fast spring and it can describe both the original curve and the working curve with the fast spring, slow spring and non-linear ratchet element.

The main equations describing this model are the following:

$$\varepsilon = \varepsilon_e + \varepsilon_v \quad (5)$$

$$\varepsilon_v = \varepsilon_p + \varepsilon_s \quad (6)$$

$$\Sigma = \Sigma_v + \Sigma_2 \quad (7)$$

$$\text{with } \Sigma = \mathrm{i}(\varepsilon_e)(8) \text{ and } \Sigma_2 = s(\varepsilon_s)(9) \text{ and } \Sigma_v = v\left(\dot{\varepsilon_v}, \varepsilon_v\right)(10)$$

$$\text{with } \Sigma_2 \leq p(\varepsilon_p)\ (11) \text{ and } \dot{\varepsilon_p} \geq 0\ (12)$$

$$\text{and } \dot{\varepsilon_p} \cdot [\Sigma_2 - p(\varepsilon_p)] = \dot{\varepsilon_p} \cdot [\Sigma_2 - \dot{p}(\varepsilon_p)] = 0 \quad (13)$$

Where ε and Σ are the strain and the specific stress of the model, respectively. $\mathrm{i}(x)$, $\mathrm{s}(x)$, $\mathrm{p}(x)$ and $\mathrm{v}(x,y)$ are non-linear real functions of real variables. $\dot{\varepsilon_v}$ and $\dot{\varepsilon_p}$ are the rates or time derivatives of

viscous strain ε_v and plastic strain ε_p. Equations (11,12,13) constitute the classical Kuhn-Tucker conditions for elastoplastic models (see Figure 14).

Each element and its method of identification will be described in the following sections.

3.1 Dynamic non-linear elasticity

Short term elasticity can be observed at high frequencies, high strain rates or during sudden changes in the loading. Looking at the multi-relaxation curve in Figure 5, we can observe short term elasticity at every re-loading after a relaxation, a creep or a recovery. It has been shown by Bles *et al* on a woven fiber strap, that the tangent modulus, just after these stages (named E_{inst} in Figure 7) , can be considered as a short-term elasticity (Bles *et al* 2009). This modulus is the equivalent of the fast spring in Flory's model during unloading. In the proposed model, this dynamic non-linear elasticity is represented by the fast spring i(ε_e).

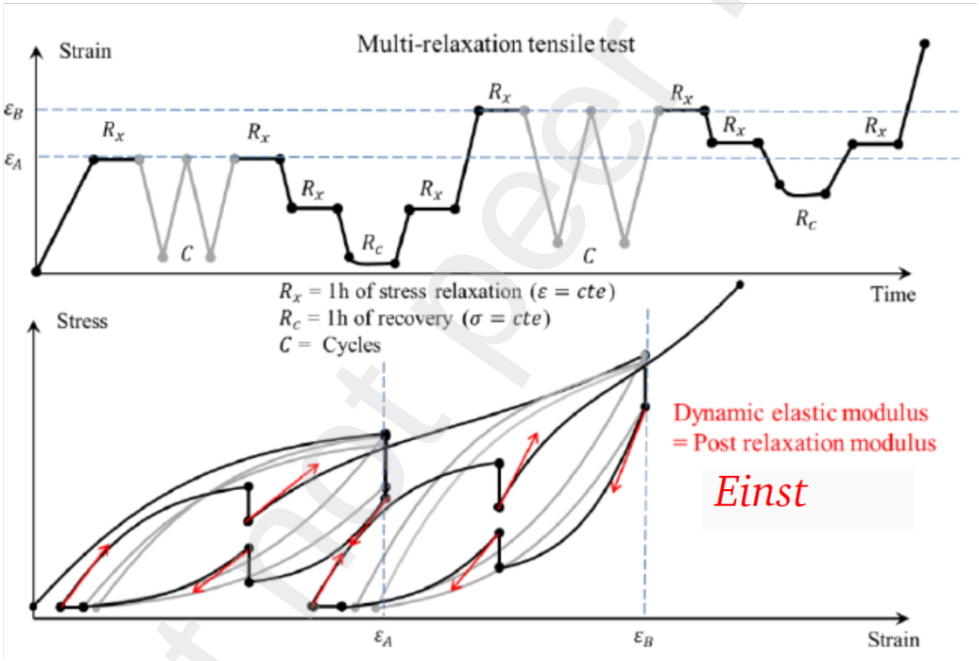

Figure 7 - Method for measuring the short-term elastic modulus

The method to measure this modulus is described in Figure 7. These moduli are plotted versus the specific stress on Figure 8, for a 4T sub-rope. We observe the short-term modulus is linear with the specific stress. On Figure 8, we do not see a clear difference between the loading and the unloading. Hence, we will assume the evolution of this modulus as a function of the specific stress is similar for both loading and unloading.

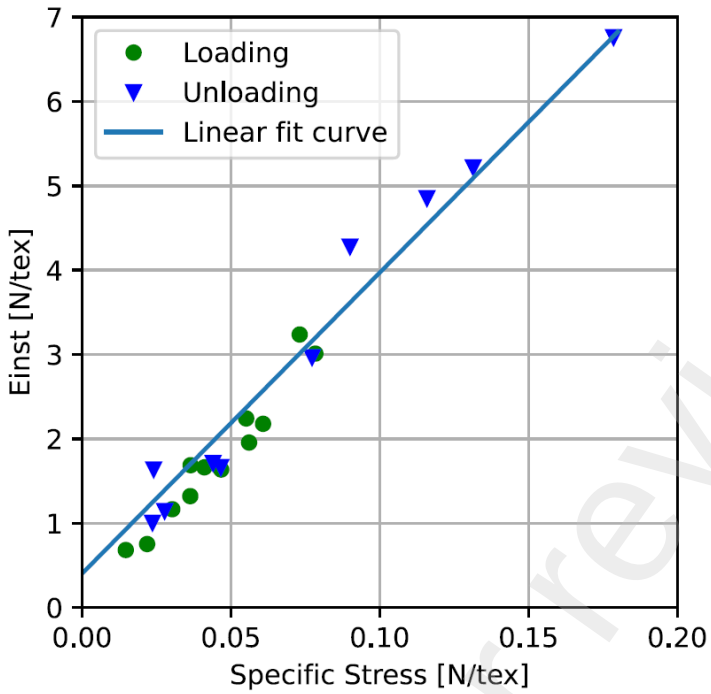

Figure 8 - Short-term elasticity modulus (E_{inst}) versus the specific stress at the beginning of the sudden change, i.e. at every re-loading after a relaxation, a creep or a recovery, for sub-rope 4T

This result is in accordance with the work of François and Davies who found the dynamic stiffness to be linear with the mean load for polyester mooring lines (François and Davies, 2008). It also confirms that the dynamic elasticity is not impacted by the history of loading. This result can be expressed as:

$$E_{inst} = a \cdot \Sigma + b = \frac{d\Sigma}{d\varepsilon}$$

Hence, we can define a function $\Sigma = i(\varepsilon)$ describing this nonlinear elasticity:

$$\Sigma = i(\varepsilon) = \frac{b}{a} \cdot \left(e^{a \cdot \varepsilon} - 1\right) \quad (14)$$

Where a has no units and b is in N/tex. These parameters can be easily identified by applying a simple linear regression to the data of Figure 8.

3.2 Fully relaxed behavior

François and Davies defined a fully relaxed behavior (FRB) (François and Davies, 2008). This behavior should include all the time-independent behavior contributions, which are: the relaxed nonlinear elasticity and the plasticity. Since it is not possible to obtain a fully relaxed state which, theoretically, would require an infinite relaxation time, we assume the following hypothesis: we observe at the end of some periods R_x on Figure 4, that when two relaxations are at the same strain (one during the

loading and the other during the unloading), a fully relaxed state may be defined by extending the two time evolutions of the stress relaxation until they meet each other (see scheme on Figure 9).

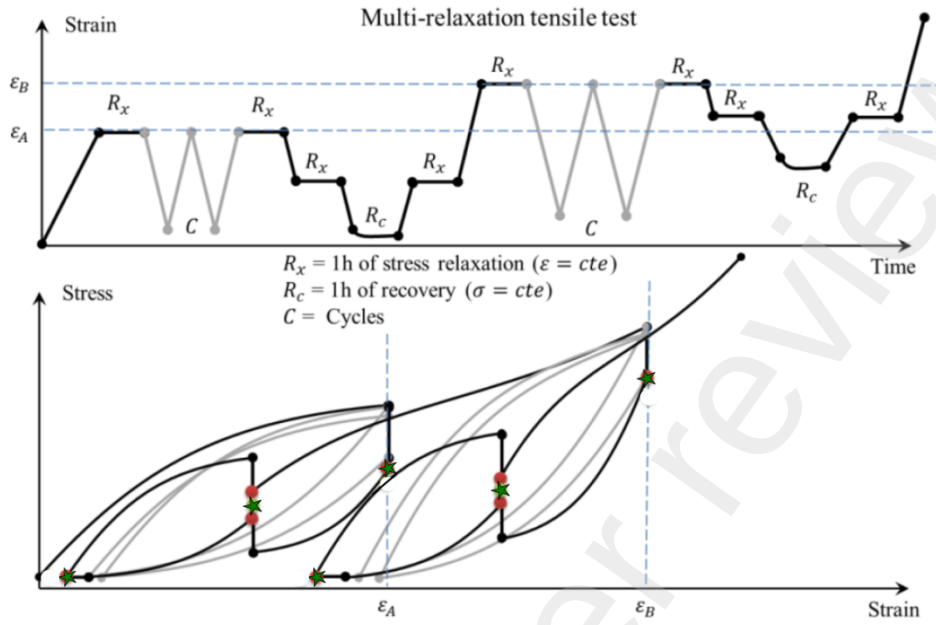

Figure 9 - Method for measuring the fully relaxed state (FRB)

Hence, a fully relaxed mechanical state can be associated to the stress values at the meeting points between two associated relaxations (green stars on Figure 9). The loading curve corresponds to the first loading of the rope and is highlighted by a continuous blue line on Figure 10. There is no opposite relaxation for the relaxations on the first loading curve or at the beginning of cycles, and there is not

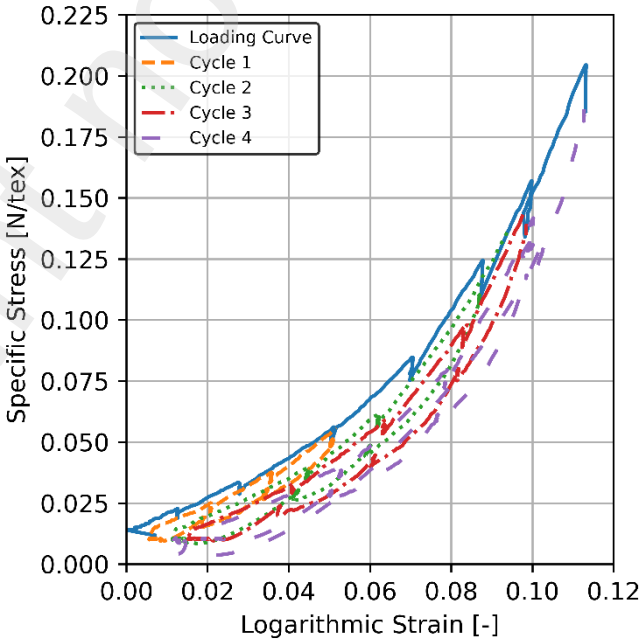

Figure 10 - Specific Stress (N/tex) versus logarithmic strain (-) during a multi-relaxation test; the blue continue line is the loading curve. The dashed lines are the cycles.

an opposite recovery for the recoveries. Hence, to a first approximation, the end of the relaxation/recovery is taken. These fully relaxed strain-stress points were measured for 4T sub-ropes and an example is given in Figure 11.

On Figure 11, we observe that the curves obtained are very similar to the ones of the Syrope model; the original working curve of the Syrope model could be compared to the first loading curve and the working curve corresponds to the FRB curves during cycles.

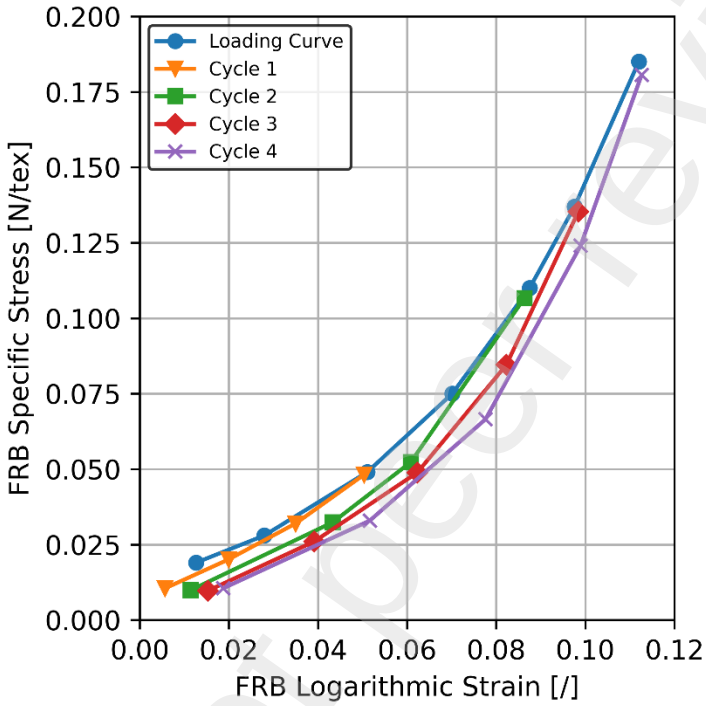

Figure 11 - Fully relaxed behavior (FRB) measured on sub-ropes 4T

This method gives an approximate value of the fully relaxed or time-independent behavior. Considering the proposed model, this behavior is revealed when the dashpot element is taken out. Only the spring and ratchet elements remain as shown on Figure 12.

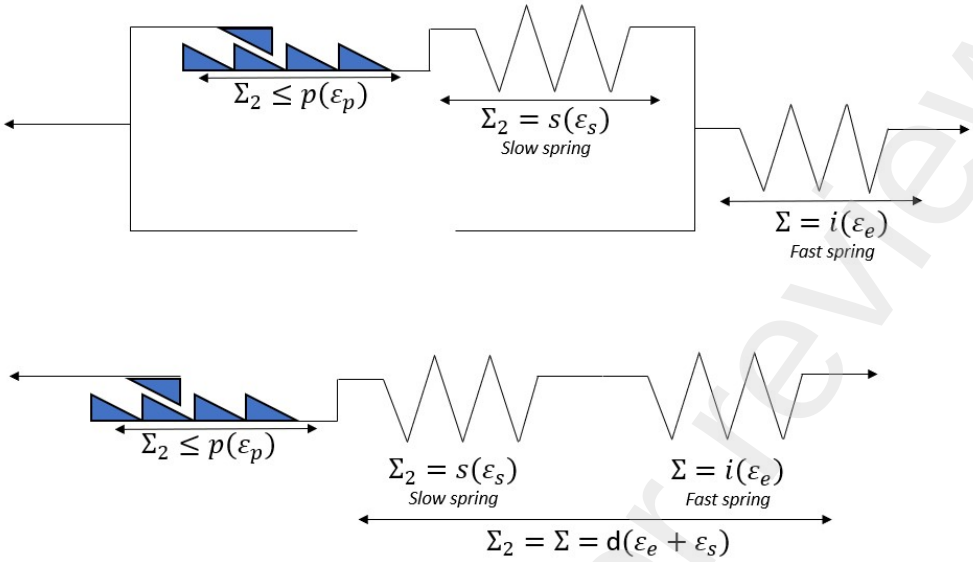

Figure 12 - POLYAMOOR model in the case of the fully relaxed behavior (when the dashpot viscosity is fully relaxed).

For the cycles of the fully relaxed behavior (not for the loading curve), a tangent modulus $M_{FRB} = \frac{d\Sigma_{FRB}}{d\varepsilon_{FRB}}$ can be determined between two measured relaxed states of the same cycle. The resulting data

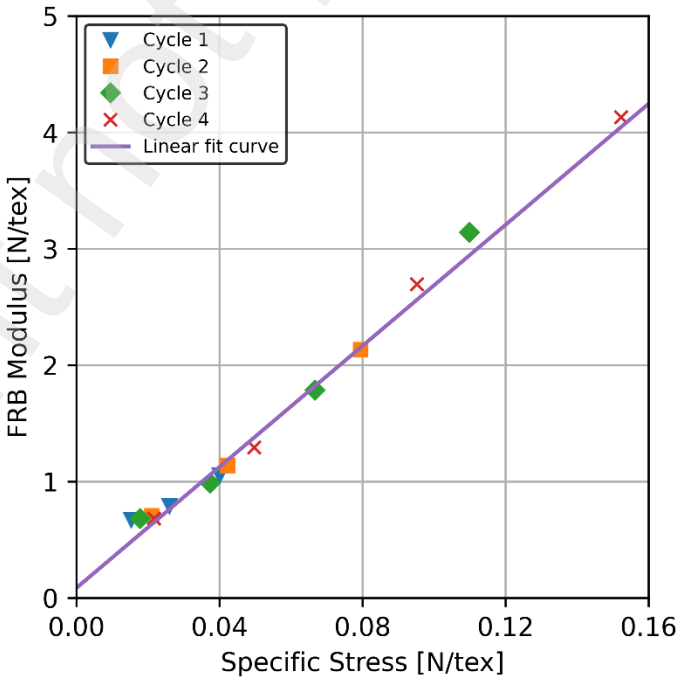

Figure 13–– Fully relaxed behavior tangent modulus $M_{FRB} = \frac{d\Sigma_{FRB}}{d\varepsilon_{FRB}}$ versus the associated specific stress for 4T sub-ropes

for a 4T sub-rope sample are presented on Figure 13; this FRB modulus is plotted versus the mean stress at the middle of two corresponding relaxed states (Figure 11).

We observe a linear relationship between this modulus and the specific stress which can be expressed as:

$$M_{FRB} = c \cdot \Sigma_{FRB} + g = \frac{d\Sigma_{FRB}}{d\varepsilon_{FRB}}$$

This is very similar to the quasi-static stiffness introduced by François and Davies who also observed it was linear with the mean load. A relationship between the stress and the strain $\Sigma_{FRB} = d(\varepsilon_{FRB})$ can consequently be found with $d(\varepsilon)$ following:

$$d(\varepsilon) = \frac{g}{c} \cdot \left(e^{c \cdot \varepsilon} - 1\right) \quad (15)$$

Parameter c has no units and g is in N/tex. These parameters can be easily identified by a simple linear regression on the cycle data of Figure 13.

As showed in Figure 12, the function $d(\varepsilon)$ describes the two springs, ('s' and 'i') , in series. So,

$$d^{-1}(\Sigma) = i^{-1}(\Sigma) + s^{-1}(\Sigma) \quad (15bis)$$

Where $f^{-1}(y)$ denotes the inverse function of a function $f(x)$. Thanks to equation 15bis and because the function $i(\varepsilon)$ was already identified, the identification of the function $d(\varepsilon)$ provides an identification of the function $s(\varepsilon)$:

$$15bis \Leftrightarrow s^{-1}(\Sigma) = d^{-1}(\Sigma) - i^{-1}(\Sigma)$$

$$\Leftrightarrow s^{-1}(\Sigma) = \frac{\ln\left(\frac{c}{g} \cdot \Sigma + 1\right)}{c} - \frac{\ln\left(\frac{a}{b} \cdot \Sigma + 1\right)}{a}$$

We inversed this function numerically using the one-dimensional Newton-Raphson algorithm.

So, at this stage, functions $i(\varepsilon)$ and $s(\varepsilon)$ are fully identified.

Once the fast elasticity and the slow elasticity are identified, we can deduce the plastic strain during the experimental test.

3.4 Plasticity

In the case of the fully relaxed behavior, the stress of the dashpot element is assumed to be zero:

$$\Sigma_v = 0$$

So

$$\Sigma_{FRB} = \Sigma_2$$

According to the model definition equations and according to equation 15bis in the FRB case, that is:

$$d^{-1}(\Sigma_{FRB}) = i^{-1}(\Sigma_{FRB}) + s^{-1}(\Sigma_{FRB}) = \varepsilon_{e\,FRB} + \varepsilon_{s\,FRB} = \varepsilon_{FRB} - \varepsilon_p$$

we have:

$$\Sigma_{FRB} = d(\varepsilon_{FRB} - \varepsilon_p)$$

For the fully relaxed cyclic behavior, this leads to the strain-stress $(\varepsilon_{FRB},\Sigma_{FRB})$ curve being shifted horizontally to the right when the plastic strain ε_p increases. Hence, on Figure 11, the curves for cycles 1, 2, 3 and 4 are described by the same modeling curve, but it is shifted from the left to the right when the maximum stress increases. This is in accordance with Figure 13 on which we can observe that the points related to the four cycles all fit the same linear function.

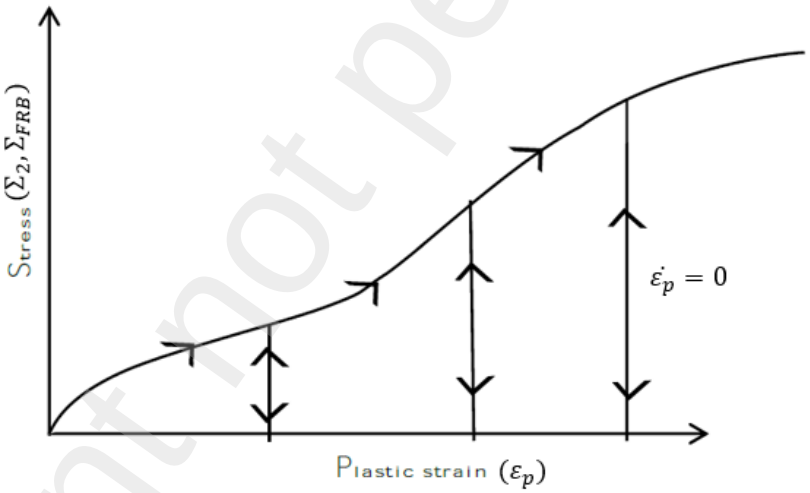

Figure 14 - Pattern of the plasticity of the fully relaxed behavior, resulting from the Kuhn-Tucker conditions as part of the proposed model definition; the plastic strain can increase only when stress $\Sigma_{FRB} = \Sigma_2$ reaches values $p(\varepsilon_p)$.

We observe that the plastic strain value increases from one cycle to another as the intersections of the curves with the plastic strain (abscissa axis) are shifted to higher values for each cycle. This identified plastic strain (ε_p) of the model may correspond to the concept of permanent elongation described by François and Davies.

Because the function $d(\varepsilon)$ has been identified previously, we can calculate the plastic strain using:

$$\varepsilon_p = \varepsilon_{FRB} - d^{-1}(\Sigma_{FRB})$$

Therefore, the plastic strain is a function of the maximum stress Σ_{FRB} as illustrated on Figure 14. Using this expression, we obtain the curve of the plastic strain against the specific stress given in Figure 15.

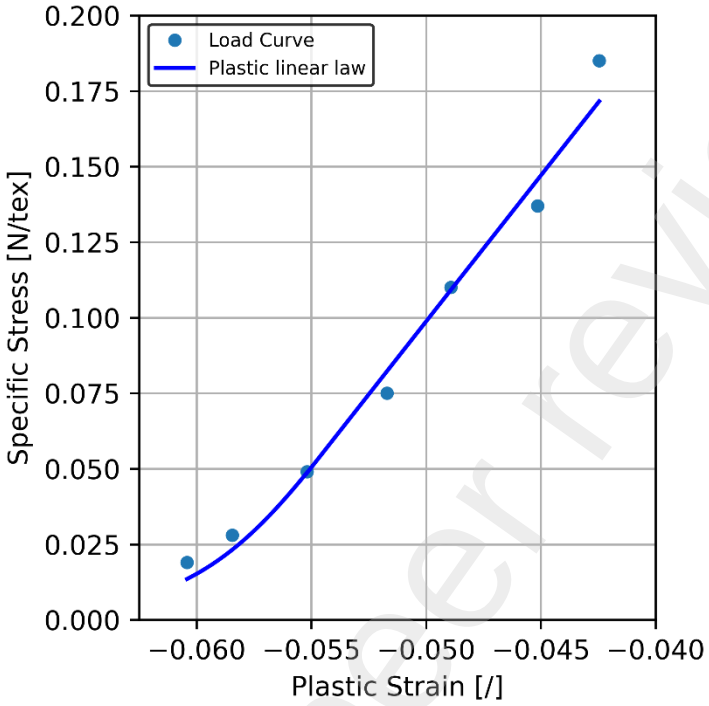

Figure 15 - Plastic strain calculated versus the specific stress, for sub-rope 4T

The negative plastic strain values obtained are due to the initial length being taken at a non-zero stress state due the need for pre-loading and a bedding-in sequence for fiber ropes as explained in section 2.4. On Figure 16, we plot the function $\Sigma_{FRB} = d(\varepsilon_{FRB} - \varepsilon_p)$ that describes the FRB behavior using the FRB strain determined for cycle 3. Figure 16 highlights how the proposed model determines a zero-specific stress for negative plastic strain values; $\Sigma_{FRB} = 0 = d(\varepsilon_{FRB} - \varepsilon_p) \Leftrightarrow \varepsilon_p = \varepsilon_{FRB}$ when $\Sigma_{FRB} = 0$.

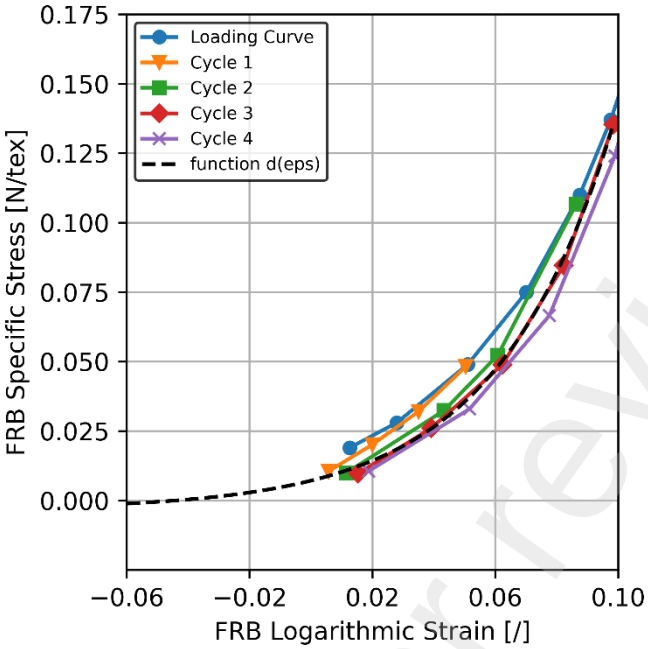

Figure 16 - Fully relaxed behavior (FRB) measured on sub-ropes 4T and function $d(\varepsilon_{FRB} - \varepsilon_p)$ plotted for cycle 3

We observe a quasi linear relation between the plastic strain and load except at the beginning of the curve. To describe as closely as possible this behavior, the function describing the plastic strain has been chosen as follows:

$$p(\varepsilon_p) = e \cdot \left(\tanh(f.\varepsilon_p + h) + 1\right) \text{ when } \varepsilon_p \leq \frac{-h}{f} \quad (16)$$

$$p(\varepsilon_p) = e \cdot (f \cdot \varepsilon_p + h + 1) \text{ when } \varepsilon_p > \frac{-h}{f} \quad (17)$$

Parameters f and h have no units while e is in N/tex. These 3 parameters can be identified by a classical one-variable function fit on the Load Curve data of Figure 15.

The only element, that remains to be identified, is the viscosity element.

3.6. Viscosity

The viscosity is represented by the dashpot, which is in parallel with the slow spring and ratchet element. We assume a nonlinear behavior of the viscosity element following the equation below inspired by the work of (François and Davies, 2008):

$$\Sigma_v = v\left(\dot{\varepsilon_v}, \varepsilon_v\right) = W_2(\varepsilon_v) \cdot \sinh^{-1}\left(\frac{\dot{\varepsilon_v}}{W_1(\varepsilon_v)}\right) \quad (19)$$

Where Σ_v and $\dot{\varepsilon_v}$ are respectively the stress and the strain rate of the viscosity element. This behavior leads to an analytical solution that can be approximated by a logarithm of the time for the relaxation. Hence, it is coherent for predicting the stress relaxation and creep strain for polyester rope which follows a logarithmic time evolution. Civier *et al* studied the creep of polyamide 6 and showed it also follows a logarithmic time evolution (Civier *et al.*, 2022).

Using the previous identification of the elastic part, the viscous strain during the experimental tests can be deduced using the expression:

$$\varepsilon = \varepsilon_e + \varepsilon_v \Leftrightarrow \varepsilon_v = \varepsilon - \varepsilon_e \Leftrightarrow \varepsilon_v = \varepsilon - i^{-1}(\Sigma) \quad (20)$$

To calculate the viscous stress, we only use the monotonic increasing plastic strain called 'load curve' on Figure 15 and highlighted on Figure 10. This means that we will only use the data from the loadings between the cycles. Hence, the obtained identification will include seven relaxations (corresponding to the seven load phases where the load exceeded the previous maximum load). Along the loading curve, the ratchet element is activated (plasticity) ($\dot{\varepsilon_p} > 0$). According to the equations of the law, the stress Σ_2 and the plastic strain satisfy the limits of relation (11):

$$\Sigma_2 = p(\varepsilon_p)$$

And according to (5) and (20) $\varepsilon_p = \varepsilon_v - \varepsilon_s = \varepsilon_v - s^{-1}(\Sigma_2) = \varepsilon - i^{-1}(\Sigma) - s^{-1}(\Sigma_2)$

So $\Sigma_2 = p(\varepsilon_v - \varepsilon_s) = p(\varepsilon_v - s^{-1}(\Sigma_2))$

$$\Leftrightarrow p^{-1}(\Sigma_2) = \varepsilon_v - s^{-1}(\Sigma_2)$$

$$\Leftrightarrow \varepsilon_v = p^{-1}(\Sigma_2) + s^{-1}(\Sigma_2)$$

We define a function k by its inverse as; $k^{-1}(\Sigma) = p^{-1}(\Sigma) + s^{-1}(\Sigma)$

So, we have: $\varepsilon_v = k^{-1}(\Sigma_2)$ (21) and $\Sigma_2 = k(\varepsilon_v)$.

According to the equations of the model (7), the viscous stress can be expressed as:

$$\Sigma_v = \Sigma - \Sigma_2 = \Sigma - k(\varepsilon_v) \quad (22)$$

$$\Leftrightarrow k(\varepsilon - i^{-1}(\Sigma)) = (\Sigma - \Sigma_v)$$

$$\Leftrightarrow \varepsilon - i^{-1}(\Sigma) = k^{-1}(\Sigma - \Sigma_v)$$

$$\Leftrightarrow \varepsilon - i^{-1}(\Sigma) - k^{-1}(\Sigma - \Sigma_v) = 0 \quad (23)$$

To calculate the viscous stress, we can use the bisection (dichotomy) method to resolve the equation (23). This method was applied to the experimental results from multi-relaxation tests on 4T sub-ropes (Figure 17).

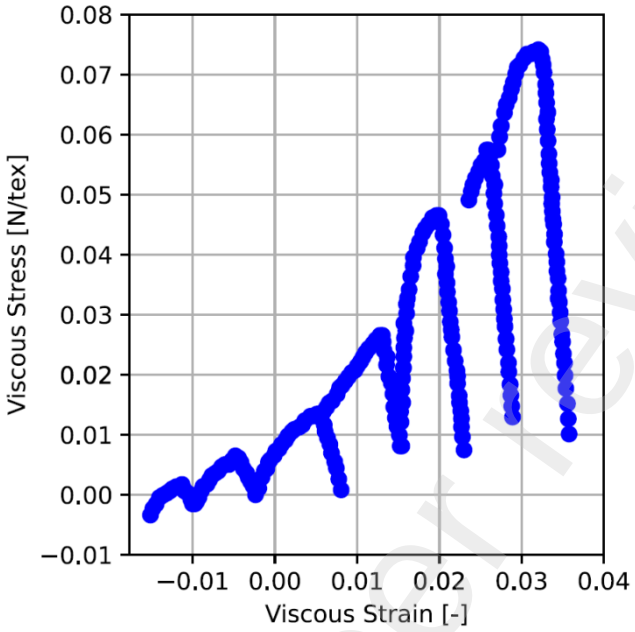

Figure 17 - Calculated viscous stress versus the viscous strain during the load curve (no cycle data) for sub-ropes 4T (the straight parts correspond to the relaxation stages of the test where the sub-rope strain is maintained constant)

To identify the parameters of the function $v(\dot{\varepsilon}_v,\varepsilon_v)$, we use the relaxation stages on Figure 17. We apply a linear regression between the viscous stress and the viscous strain for each relaxation stage:

$$\Sigma_v = -r \cdot \varepsilon_v + q \quad (23bis)$$

The chosen viscosity behavior, added to this linear relation, led to the following differential equation:

$$\dot{\varepsilon}_v = W_1 \cdot \sinh\left(\frac{-r \cdot \varepsilon_v + q}{W_2}\right) \quad (24)$$

We resolve it analytically giving:

$$\Sigma_v(t) = 2 \cdot W_2 \cdot \tanh^{-1}\left[\tanh\left(\frac{\Sigma_v(t_0)}{2 \cdot W_2}\right) \cdot \exp\left(\frac{-r \cdot W_1.(t - t_0)}{2 \cdot W_2}\right)\right] \quad (25)$$

In this equation resulting from the behavior of the model, $\Sigma_v(t)$ is given by the data of Figure 17, and the parameter r is given by the linear regression (eq.23bis). So we can optimize parameters W_1 and W_2 for a best fit on experimental data of each relaxation stage on Figure 17 (7 stages). This

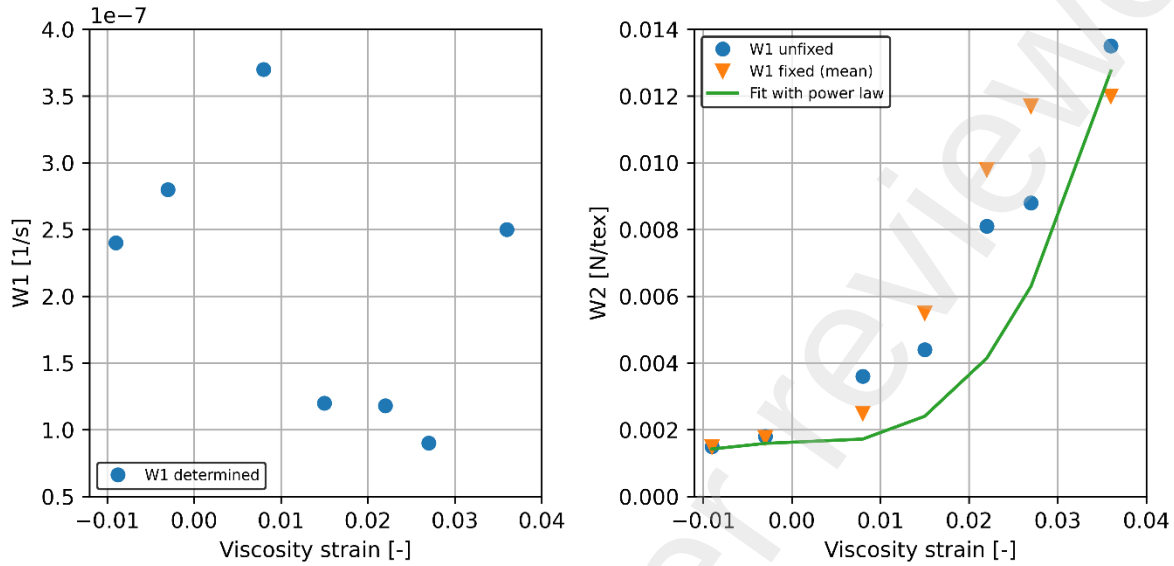

Figure 18 - Parameters W1 and W2 calculated from the viscosity behavior for 4T sub-ropes sample

optimization was done by a non-linear least-squares Marquardt-Levenberg algorithm applied to the equation (25). Figure 18 presents these values versus the mean value of the viscous strain during the relaxation stages.

According to experimental observations (Figure 18-left), W1 does not show a simple variation depending on the viscous strain and the variations are small with respect to those of W2, resulting in a low contribution to the overall viscous strain. So, we decided to fix W1 as a constant (equal to the mean of the values obtained) and not as a function of the viscous strain. Using a fixed value for W1 we can apply the non-linear least-squares Marquardt-Levenberg algorithm again to optimize W2. Figure 18-right shows the W2 values obtained both using a fixed value for W1 (triangle) or unfixed values (circle). Also Figure 19 shows the evolution of the specific viscous stress for three different relaxations (different initial specific stress at the beginning of the relaxation) using fixed W1 values or using W1 values unfixed. The differences are small, so the choice of a fixed value allows us to simplify the law and seems appropriate.

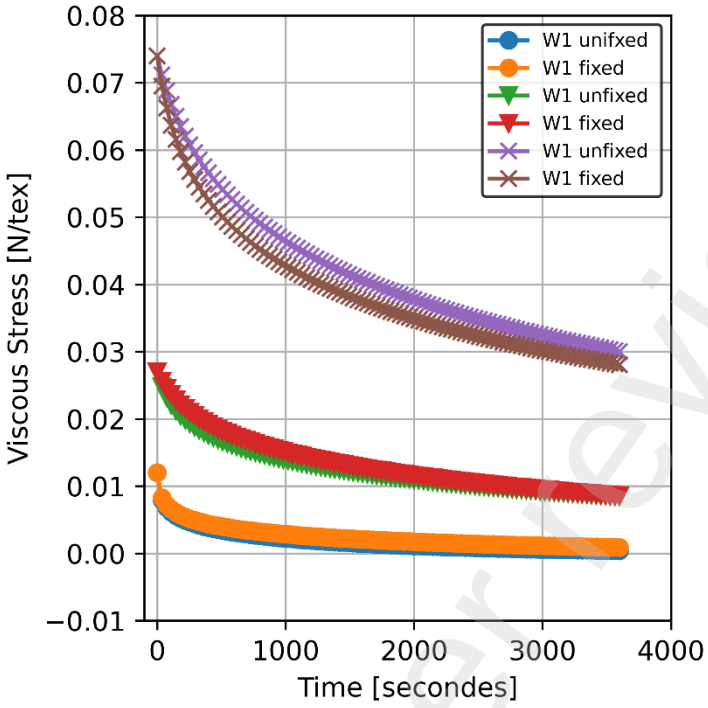

Figure 19 - Evolution of the specific viscous stress (N/tex) following equation 25 for three different relaxations (circles, triangle, cross) using W1 fixed or unfixed

The W2 behavior with respect to the viscous strain can be expressed using a power law:

$$W_2(\varepsilon_v) = a_{w2} \cdot \varepsilon_v^{\alpha} + b_{w2} \quad (26)$$

With a_{w2} and b_{w2} expressed in N/tex and α with no units.

4. Parameter identification and experimental validation

4.1 Identification, simulation by finite element analysis and experimental validation for the 4T sub-rope sample

Following the identification method, the 11 parameters of the POYLAMOOR model were identified using the multi-relaxation data of four tests on 4T sub-rope samples as described above. For each parameter, the average of the parameters obtained for the four tests was calculated. These are presented in Table 2. An example of the experimental plots is shown on Figure 5.

Table 2 - Identified parameters for the POLYAMOOR on a 4T sub-rope sample

	4T value	Element of the POLYAMOOR model
a [-]	33	$i(\varepsilon) = \frac{b}{a} \cdot (e^{a \cdot \varepsilon} - 1)$
b [N/tex]	0.48	
c [-]	26	$d(\varepsilon) = \frac{g}{c} \cdot (e^{c \cdot \varepsilon} - 1)$
g [N/tex]	0.086	
e [N/tex]	0.11	$p(\varepsilon_p) = e \cdot (\tanh(f \cdot \varepsilon_p + h) + 1)$ if $\varepsilon_p \leq \frac{-h}{f}$
f [-]	161	$p(\varepsilon_p) = e \cdot (f \cdot \varepsilon_p + h + 1)$ if $\varepsilon_p > \frac{-h}{f}$
h [-]	8	
W_1 (s^{-1})	$1.8 \cdot 10^{-7}$	$\Sigma_v = v(\dot{\varepsilon_v}, \varepsilon_v) = W_2(\varepsilon_v) \cdot \sinh^{-1}\left(\frac{\dot{\varepsilon_v}}{W_1}\right)$
α [-]	3	$W_2(\varepsilon_v) = a_{w2} \cdot \varepsilon_v^{\alpha} + b_{w2}$
a_{W2}[N/tex]	186.75	
b_{w2} [N/tex]	0.0016	

A validation of the approach was performed by comparing the simulation of this experimental procedure using the parameters in Table 2 to the experimental data. The behavior given by the model is very close to the experimental response (Figure 20 and Figure 21).

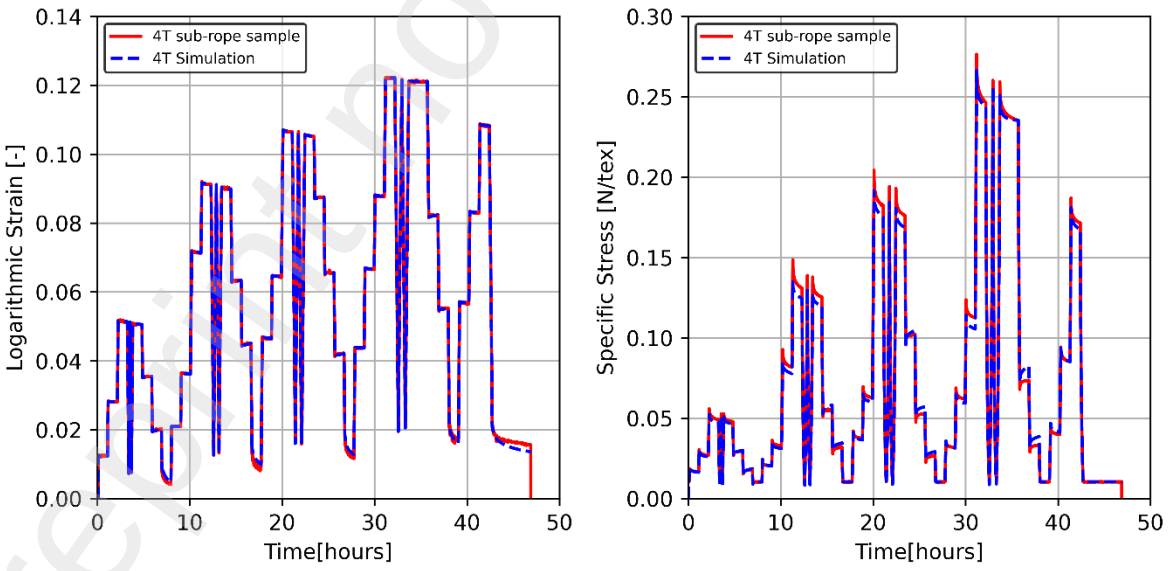

Figure 20- Comparison of the model and the experimental results for the 4T sample Left: Time evolution of the logarithmic strain [-] for the experimental result and the model Right: Time evolution of the specific stress [N/tex]

Some differences can be seen for the recoveries but they are quite small. We observe on Figure 20-right and Figure 21-right that the model under and overestimates the specific stress during the loading and the unloading, respectively. This error could, in part, be explained by the hypothesis of linear

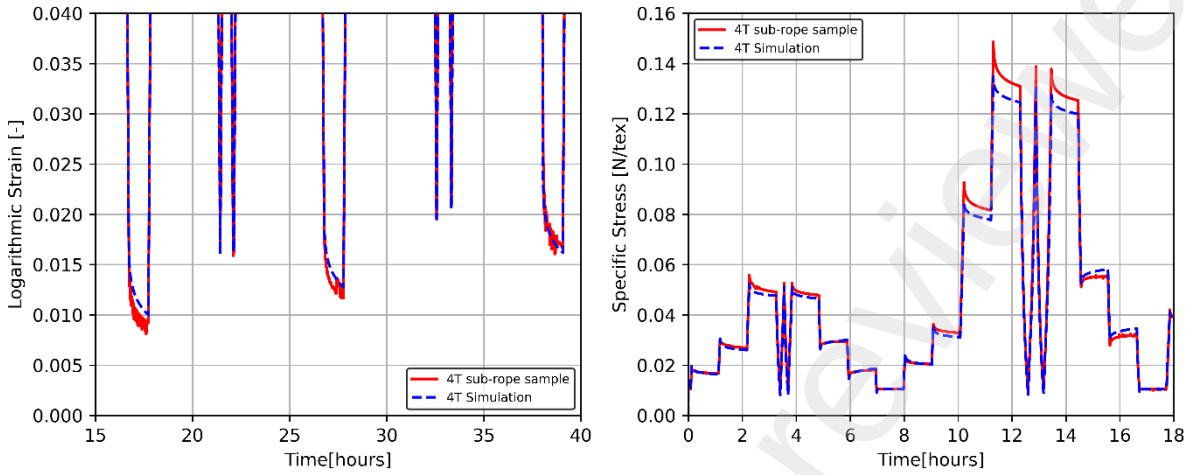

Figure 21 - Zoom of the figure 20: Left: Evolution of the logarithmic strain Right: Evolution of the specific stress

evolutions of the moduli versus the specific stress for the loading and the unloading. This linearity during the loading may not be completely justified, as we see the model fits the experimental data well for cycle 1 and 4 and underestimates it for cycle 2 and 3. It could also be due to an underestimated evolution of the specific stress in the ratchet element. The parameters could be optimized to describe a chosen load range more closely. Such an optimization should be performed on all parameters, as their identification is inter-dependent.

There is a visible difference in the behavior during the relaxations at unloading. This was expected as the viscous parameters have been identified on the first loading sequence of the test and we can expect some differences between the loading and the unloading steps. The choice of equation (19) to describe the viscosity behavior could also be questioned and another behavior might improve the prediction.

Overall, the model works well with cycles and relaxations in the load range of 0.01 to 0.25 N/tex for the 4T sub-rope sample. The differences are not critical for the application. The POLYAMOOR model should allow the behavior of mooring lines under normal service loading (cycle 1 reaches 0.1 N/tex around 17%MBL) and under storm conditions (cycle 4 reaches 0.45 N/tex around 77%MBL) to be determined.

5. Conclusion

A constitutive model based on Flory's proposal and its identification method was proposed. It does not require any inverse identification and allows good control over the model. The model reproduces

both the concepts of permanent elongation and creep behavior introduced respectively by Francois *et al* and Civier *et al*. The model has been defined such that it can be implemented in a one-dimensional FEM model solved in the time domain, assuming access to stored mechanical parameters of the global numerical scheme.

This model was developed using a cyclic multi-relaxation test which can be applied to the prediction of the mechanical behavior of polyamide 6 fiber ropes under representative loading. It has the following elements:

- A fast spring describing the dynamic behavior,
- A dashpot responsible for the viscous stress of the polymer,
- A time-independent part consisting of a ratchet element for the plasticity, and a slow spring responsible for the relaxed elasticity.

A first validation has been made by comparing the model results to the experimental data used for the identification. The model predicts some small differences as it under or overestimates the specific stress during some cycles. Also, some differences on the recovery stages are visible but remain small. The viscous expression is suspected to be the source of differences and further work may allow optimization of this component. Nevertheless, these differences are instantaneous and do not affect the remaining loading history. Hence, it was concluded that the differences were not critical for the application and that further optimization of the parameters could allow a correction of the model if needed.

Further validations are being made by applying the law and the identified parameters to other loading sequences, in order to show whether the law can be predictive.

As the development of the law was made on 4T sub-rope samples, an identification of the law at higher scales is on-going. The aim of those identifications is to investigate if larger scale ropes, composed of the same fibers but with a different construction, show a similar response to the one identified on the 4T sub-rope. The analysis of the parameters obtained will also enable the influence of the rope construction to be investigated.

6. Acknowledgements

This work was performed within the FEM/ANR POLYAMOOR and MONAMOOR projects of the French national research agency project (ANR-10-IEED-0006-16 and ANR-10-IEED-06-34, Investissements d'Avenir). This is led by France Energies Marines with partners Bureau Veritas, BEXCO Ropes, ENSTA Bretagne, IFREMER, Naval Energies, Saipem, Total Energies, University of Nantes, University Gustave Eiffel, NCD, IFSTTAR, GeM, CNRS, WEAMEC and RWE. Thanks also to the engineering and technical

staff team, without whom this study would not have been possible: Sébastien Bourc'his, Raphael Poncin, Didier Penchenat, Bruno Mecucci and Eric Saliou.

7. References

Bain, C., Davies, P., Bles, G., Marco, Y., Barnet, J., 2020. Influence of bedding-in on the tensile performance of HMPE fiber ropes. Ocean Eng. 203, 107144. https://doi.org/10.1016/j.oceaneng.2020.107144

Bles, G., Nowacki, W.K., Tourabi, A., 2009. Experimental study of the cyclic visco-elasto-plastic behaviour of a polyamide fibre strap. Int. J. Solids Struct. 46, 2693–2705. https://doi.org/10.1016/j.ijsolstr.2009.02.015

Chailleux, E., Davies, P., 2005. A Non-Linear Viscoelastic Viscoplastic Model for the Behaviour of Polyester Fibres. Mech. Time-Depend. Mater. 9, 147–160. https://doi.org/10.1007/s11043-005-1082-0

Chailleux, E., Davies, P., 2003. Modelling the Non-Linear Viscoelastic and Viscoplastic Behaviour of Aramid Fibre Yarns. Mechanics of Time-Dependent Materials 291, 291–303.

Chevillotte, Y., 2020. Characterization of the long-term mechanical behavior and the durability of polyamide mooring ropes for floating wind turbines. ENSTA Bretagne/ Université Bretagne Loire, Brest, France.

Civier, L., Chevillotte, Y., Bles, G., Montel, F., Davies, P., Marco, Y., 2022. Short and long term creep behaviour of polyamide ropes for mooring applications. Ocean Eng. 259, 111800. https://doi.org/10.1016/j.oceaneng.2022.111800

Davies, P., Chailleux, E., Bunsell, A., Grosjean, F., Francois, M., 2003. Prediction of the long term behavior of synthetic mooring lines, in: All Days. OTC, Houston, Texas, p. OTC-15379-MS. https://doi.org/10.4043/15379-MS

Durville, D., 2002. Modélisation par éléments finis du comportement mécanique de structures textiles : de la fibre au tissu. Rev. Eur. Éléments Finis 11, 463–477. https://doi.org/10.3166/reef.11.463-477

Falkenberg, E., Åhjem, V., Yang, L., 2017. Best Practice for Analysis of Polyester Rope Mooring Systems, in: Day 3 Wed, May 03, 2017. OTC, Houston, Texas, USA, p. D031S034R006. https://doi.org/10.4043/27761-MS

607 Flory, J.F., Ahjem, V., Banfield, S.J., 2007. A New Method of Testing for Change-in-Length Properties
608 of Large Fiber-Rope Deepwater Mooring Lines, in: All Days. OTC, Houston, Texas, U.S.A., p.
609 OTC-18770-MS. https://doi.org/10.4043/18770-MS
610
611 Flory, John F., Banfield, S.J., Berryman, C., 2007. Polyester Mooring Lines on Platforms and MODUs in
612 Deep Water, in: All Days. OTC, Houston, Texas, U.S.A., p. OTC-18768-MS.
613 https://doi.org/10.4043/18768-MS
614
615 François, M., Davies, P., 2008. Characterization of Polyester Mooring Lines, in: Volume 1: Offshore
616 Technology. ASMEDC, Estoril, Portugal, pp. 169–177. https://doi.org/10.1115/OMAE2008-
617 57136
618
619 Ghoreishi, S.R., Cartraud, P., Davies, P., Messager, T., 2007. Analytical modeling of synthetic fiber ropes
620 subjected to axial loads. Part I: A new continuum model for multilayered fibrous structures.
621 Int. J. Solids Struct. 44, 2924–2942. https://doi.org/10.1016/j.ijsolstr.2006.08.033
622
623 Huang, W., Liu, H., Lian, Y., Li, L., 2015. Modeling nonlinear time-dependent behaviors of synthetic
624 fiber ropes under cyclic loading. Ocean Eng. 109, 207–216.
625 https://doi.org/10.1016/j.oceaneng.2015.09.009
626
627 Huang, W., Liu, H., Lian, Y., Li, L., 2013. Modeling nonlinear creep and recovery behaviors of synthetic
628 fiber ropes for deepwater moorings. Appl. Ocean Res. 39, 113–120.
629 https://doi.org/10.1016/j.apor.2012.10.004
630
631 Humeau, C., Davies, P., LeGac, P.Y., Jacquemin, F., 2018. Influence of water on the short and long term
632 mechanical behaviour of polyamide 6 (nylon) fibres and yarns. Multiscale Multidiscip. Model.
633 Exp. Des. 1, 317–327. https://doi.org/10.1007/s41939-018-0036-6
634
635 Huntley, M.B., 2016. Fatigue and modulus characteristics of wire-lay nylon rope, in: OCEANS 2016
636 MTS/IEEE Monterey. IEEE, Monterey, CA, USA, pp. 1–6.
637 https://doi.org/10.1109/OCEANS.2016.7761501
638
639 Lechat, C., Bunsell, A.R., Davies, P., Piant, A., 2006. Mechanical behaviour of polyethylene
640 terephthalate & polyethylene naphthalate fibres under cyclic loading. J. Mater. Sci. 41, 1745–
641 1756. https://doi.org/10.1007/s10853-006-2372-x
642
643 Lian, Y, 2018. An experimental investigation on the bedding-in behavior of synthetic fiber ropes. Ocean
644 Eng. 160, 368–381. https://doi.org/10.1016/j.oceaneng.2018.04.071
645
646 NI 432 Dt R02 E Bureau Veritas, 2007. Certification of Fibre Ropes for Deepwater Offshore Services.
647 (Technical Report).

Pham, H., Cartraud, P., Schoefs, F., Soulard, T., Berhault, C., 2019. Dynamic modeling of nylon mooring lines for a floating wind turbine. Appl. Ocean Res. 87, 1–8. https://doi.org/10.1016/j.apor.2019.03.013

Sorum, S.H., Fonseca, N., Kent, M., Faria, R.P., 2023. Modelling of Synthetic Fibre Rope Mooring for Floating Offshore Wind Turbines. J. Mar. Sci. Eng. 11, 193. https://doi.org/10.3390/jmse11010193

Weller, S.D., Banfield, S.J., Canedo, J., 2018. Parameter Estimation for Synthetic Rope Models, in: Volume 1: Offshore Technology. American Society of Mechanical Engineers, Madrid, Spain, p. V001T01A072. https://doi.org/10.1115/OMAE2018-78606

Weller, S.D., Johanning, L., Davies, P., Banfield, S.J., 2015. Synthetic mooring ropes for marine renewable energy applications. Renew. Energy 83, 1268–1278. https://doi.org/10.1016/j.renene.2015.03.058